Finite-Control-Set Model-Predictive Control for a Quasi-Z-Source Four-Leg Inverter Under Unbalanced Load Condition

Sertac Bayhan, *Member, IEEE*, Mohamed Trabelsi, *Member, IEEE*, Haitham Abu-Rub, *Senior Member, IEEE*, and Mariusz Malinowski, *Fellow, IEEE*

***Abstract*—This paper presents finite-control-set model-predictive control (FCS-MPC) for a three-phase quasi-Z-source (qZS) four-leg inverter under unbalanced load condition. The key novelty of the proposed control approach is eliminating the double-line frequency ripple in the inductor current with a simple and effective approach. The proposed four-leg qZS inverter with an output LC filter can handle buck/boost and dc/ac conversion features in a single stage. Furthermore, the FCS-MPC-based control algorithm helps in maintaining balanced point of common coupling voltages for stand-alone unbalanced loads. The behavior of the predictive controller has been investigated under different operating conditions, and its robustness with the qZS network and the LC filter parameter variations are also studied. Furthermore, the effect of double-line frequency ripple and its relation with the inductor current constraint have been tackled comprehensively. To verify the performance of the proposed approach, simulation and experimental studies were performed for balanced and unbalanced loads.**

***Index Terms*—DC–AC power conversion, digital control, model-predictive control, quasi-Z-source inverter (qZSI).**

I. Introduction

INSTALLING stand-alone power systems in off-grid locations has been receiving much attention recently due to their considerable advantages. They are most often used in remote areas where electricity is not available or where the connection fees of the utility grid are very expensive such as remote villages, islands, ship propulsion systems, and large communities [1]. In such systems, power converters play a critical role in supplying constant and smooth voltage to the local loads that can be single-/three-phase and balanced/unbalanced loads.

Various power electronic converter topologies have been proposed in the literature for the renewable-energy-source-based stand-alone applications. Typically, these are divided into two main categories: dual-stage (with dc/dc converter) and single-stage (without dc/dc converter). Each of these categories may contain galvanically isolated or nonisolated topologies, among other features. The single-stage inverter topology offers advantages over the dual-stage that include a lower number of active semiconductor switches, higher efficiency, and increased reliability [2], [3]. This single-stage topology, however, must still perform the same functions as a dual-stage inverter including maximum power point tracking (MPPT), immunity to input voltage variations, and producing clean sinusoidal output current with low total harmonic distortion (THD) [4].

One of the competitive single-stage topology candidates that has received significant interest for the photovoltaic (PV) systems is the quasi-Z-source inverter (qZSI) [5], [6], a variant of the Z-source inverter. The qZSI can provide voltage buck/boost and dc/ac conversion functionality in a single stage with simple impedance ($Z = LC$) network [7].

Although the three-phase three-leg qZSI is employed in many stand-alone PV applications [8], it has some drawbacks. One of the main drawbacks of this topology is that it is designed to supply balanced three-phase loads. On the other hand, unbalanced loads can also be connected to such systems. As a result, circulating current flows throughout the power system, which results in overheat in the neutral line whereas high distortion in the output voltage [9]. To overcome these issues, a three-phase four-wire voltage-source inverter (VSI) can be used with the split dc-link capacitors. This approach is simple; however, it leads to low utilization of the dc-link voltage, and it requires two large capacitors to circumvent the current ripples [10]. To improve dc-link utilization and reduce the dc-link capacitor size, a four-leg inverter is becoming an attractive solution for the three-phase four-wire systems, especially where loads are unbalanced [11], [12]. The four-leg inverter topology can be employed in many applications that include stand-alone PV systems [13], uninterruptible power supplies [14], and dynamic voltage restorers [15].

Similar to the traditional single-phase inverter, the double-line frequency ($2f_o$) power flows through the dc link of the

Manuscript received May 31, 2016; revised August 4, 2016 and October 3, 2016; accepted October 22, 2016. Date of publication November 22, 2016; date of current version March 8, 2017. This work was supported by NPRP-EP X-033-2-007 (Sections I and II) and NPRP 8-241-2-095 (Sections III, IV, and V) from the Qatar National Research Fund (a member of the Qatar Foundation). The statements made herein are solely the responsibility of the authors.

S. Bayhan is with the Department of Electronics and Automation, Gazi University, Ankara 06560, Turkey, and also with the Department of Electrical and Computer Engineering, Texas A&M University at Qatar, Doha 23874 Qatar (e-mail: sbayhan@gazi.edu.tr).

M. Trabelsi and H. Abu-Rub are with the Department of Electrical and Computer Engineering, Texas A&M University at Qatar, Doha 23874 Qatar (e-mail: mohamed.trabelsi@qatar.tamu.edu; haitham.abu-rub@qatar.tamu.edu).

M. Malinowski is with the Department of Electrical Engineering, Warsaw University of Technology, Warsaw 00-662 Poland (e-mail: malin@isep.pw.edu.pl).

Color versions of one or more of the figures in this paper are available online at http://ieeexplore.ieee.org.

Digital Object Identifier 10.1109/TIE.2016.2632062

quasi-Z-source (qZS) four-leg inverter in case of unbalanced output current condition. This leads to $2f_o$ voltage ripple of the dc link and capacitor and $2f_o$ current ripple of impedance network inductors. Most particularly, high $2f_o$ current ripple in the inductor results in high hysteresis losses, which reduces the overall system efficiency. One way to minimize the $2f_o$ ripple in the current is to use a large inductance, which considerably increases the inverter size, weight, and cost. For that reason, using such a system under unbalanced load condition requires special control techniques to reduce or eliminate $2f_o$ ripple in the dc-link voltage and current.

The control of power electronic converters plays an important role to ensure good transient response with high accuracy in steady-state operation. However, those are still problematic issues of the classical linear controllers [16]–[18]. Moreover, the classical linear controllers require an additional modulation stage to generate the gate signals for power switches, which often would be complex in nature [19]–[22]. For that reason, their limitations should be considered when applied to the qZSIs and four-leg inverters.

A finite-control-set model-predictive control (FCS-MPC) technique is appeared as a new control approach for power electronic converters due to its considerable benefits such as easy implementation, flexibility, and nonlinearities in the cost function [23], [24]. FCS-MPC is also straightforward to implement and provides the ability to incorporate various operational variables and constraints without structural changes in the main control design [25], [26]. The FCS-MPC has been successfully applied for different types of power electronic applications [27]–[31].

A predictive control technique for a four-leg qZSI was presented in [32] with limited simulation results. Furthermore, in [32], the output current and capacitor voltages were controlled without taking into consideration double-line frequency ripples in the case of unbalanced load condition. On the other hand, this paper provides a comprehensive FCS-MPC-based control algorithm, which eliminates $2f_o$ ripple in the inductor current. The proposed control approach improves the overall system performance compared to previous work. Simulation and experimental investigations are conducted to verify the proposed system performance. The main contributions of this study are summarized as follows.

1) The advantages of qZSI and four-leg inverter topology are combined together to obtain a robust and effective single-stage power converter for stand-alone applications.
2) The load voltage is controlled instead of the load current. Thus, the proposed system is suitable for the stand-alone applications.
3) The input current is controlled to mitigate the double-line ($2f_o$) frequency ripple in the inductor current, which leads to significant reduction of the input stress without using additional passive or active techniques. As a result, the size and cost of the inverter is decreased.
4) The robustness of the proposed controller is studied with parameters variations.

This paper is organized as follows. In Section II, the continuous time model and operating principle of the qZS four-leg inverter are presented. The proposed FCS-MPC strategy is described in Section III. The simulation and experimental results are presented together in Section IV. Finally, conclusions are given in Section V.

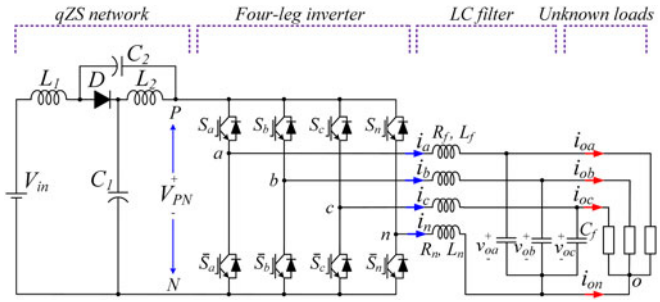

Fig. 1. Quasi-Z source three-phase four-leg inverter with an output LC filter.

TABLE I
SWITCHING STATES OF THE THREE-PHASE FOUR-LEG INVERTER WITH SHOOT-THROUGH STATE

Switching State		Sa	S′a	Sb	S′b	Sc	S′c	Sn	S′n
Non-shoot-through states	0	1	0	0	1	0	1	0	1
	1	1	0	1	0	0	1	0	1
	2	0	1	1	0	0	1	0	1
	3	0	1	1	0	1	0	0	1
	4	0	1	0	1	1	0	0	1
	5	1	0	0	1	1	0	0	1
	6	1	0	1	0	1	0	0	1
	7	0	1	0	1	0	1	0	1
	8	1	0	0	1	0	1	1	0
	9	1	0	1	0	0	1	1	0
	10	0	1	1	0	0	1	1	0
	11	0	1	1	0	1	0	1	0
	12	0	1	0	1	1	0	1	0
	13	1	0	0	1	1	0	1	0
	14	1	0	1	0	1	0	1	0
	15	0	1	0	1	0	1	1	0
STS[1]	16	1	1	1	1	1	1	1	1

STS:shoot-through-state[1]

II. QUASI-Z-SOURCE FOUR-LEG INVERTER MODEL

Fig. 1 shows the proposed qZS four-leg inverter topology with unknown local loads. Although traditional four-leg inverter topology requires 16 switching states, the qZS four-leg inverter topology needs one more switching state to achieve boost capability. To do that, both switches in the same leg must be turned ON at the same time, which is prohibited in the traditional VSIs. The switching states are given in Table I.

A. Mathematical Model of the Quasi-Z Source Network

Mathematical models of the qZS network are summarized in this section [32]. The current and voltage labels are defined in Fig. 2(a) and (b).

The four-leg inverter can be illustrated as a constant current source in case of the nonshoot-through state [see Fig. 2(a)]. The inductor voltages (v_{L1} and v_{L2}), dc-link voltage ($v_{\rm PN}$), and diode voltage (v_{D1}) are

$$v_{L1} = V_{\rm in} - V_{C1}, \quad v_{L2} = -V_{C2} \tag{1}$$

$$v_{\rm PN} = V_{C1} - v_{L2} = V_{C1} + V_{C2}, \quad v_{\rm diode} = 0. \tag{2}$$

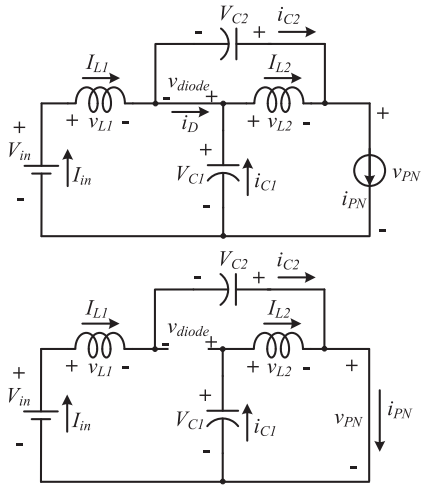

Fig. 2. Equivalent circuit of the qZS network. (a) Nonshoot-through state. (b) Shoot-through state.

On the other hand, the four-leg inverter is illustrated as short circuit in dc-link voltage, as shown in Fig. 2(b), in the case of the shoot-through state. In this case, the inductor voltages (v_{L1} and v_{L2}), dc-link voltage ($v_{\rm PN}$), and diode voltage ($v_{\rm diode}$) are

$$v_{L1} = V_{C2} + V_{\rm in},\ \ v_{L2} = V_{C1} \tag{3}$$

$$v_{\rm PN} = 0\ \ v_{\rm diode} = V_{C1} + V_{C2}. \tag{4}$$

The average capacitors voltage over one switching cycle are

$$\left.\begin{aligned} V_{C1} &= \frac{T_1}{T_1 - T_0} V_{\rm in} = mV_{\rm in} \\ V_{C2} &= \frac{T_0}{T_1 - T_0} V_{\rm in} = nV_{\rm in} \end{aligned}\right\} \tag{5}$$

where T_0 is the duration of the shoot-through state, T_1 is the duration of the nonshoot-through state, and $V_{\rm in}$ is the input dc voltage. Here, $m > 1$ and $m - n = 1$. From (2), (4), and (5), the peak dc-link voltage across the inverter bridge is given by

$$v_{\rm PN} = V_{C1} + V_{C2} = \frac{T}{T_1 - T_0} V_{\rm in} = BV_{\rm in} \tag{6}$$

where T is the switching cycle and B is the boost factor of the qZSI. If $B <= 1$, then the inverter works in buck mode, and if $B > 1$, then the inverter works in boost mode. From (5), B can be rewritten as $m + n = B$, and $1 < m < B$.

The average current of inductors L_1 and L_2 can be calculated by the inverter power rating P

$$I_{L1} = I_{L2} = I_{\rm in} = P/V_{\rm in}. \tag{7}$$

According to Kirchoff's current law and (7), we can also obtain that

$$i_{c1} = i_{c2} = i_{\rm PN} - I_{L1}. \tag{8}$$

B. Mathematical Model of the Four-Leg Inverter

Fig. 1 illustrates the four-leg inverter topology with an output LC filter. In this configuration, the neutral point of the load and the star point of C filter are connected to the fourth leg through a neutral inductor (L_n). Although using one extra leg increases the complexity of the inverter, it provides the zero-sequence voltage control capability for the unbalanced loads. Furthermore, using L_n reduces the switching frequency ripples in the neutral current (i_n) [33]. It can be noticed that the inverter neutral point is depicted as n, whereas the load neutral point is depicted as o. To simplify the analysis, the following voltage and current vectors are defined:

$$\left.\begin{aligned} \mathbf{v} &= \begin{bmatrix} v_{\rm an} & v_{\rm bn} & v_{\rm cn} \end{bmatrix}^T \\ \mathbf{v_o} &= \begin{bmatrix} v_{\rm oa} & v_{\rm ob} & v_{\rm oc} \end{bmatrix}^T \\ \mathbf{i} &= \begin{bmatrix} i_a & i_b & i_c \end{bmatrix}^T \\ \mathbf{i_o} &= \begin{bmatrix} i_{\rm oa} & i_{\rm ob} & i_{\rm oc} \end{bmatrix}^T \end{aligned}\right\}. \tag{9}$$

The output voltage of the inverter is

$$v_{\rm jn} = v_{\rm jn}t - v_{\rm nN} = (S_j - S_n)\, V_{\rm nN}\, PN,\ \ j = a, b, c \tag{10}$$

where $V_{\rm PN}$ is the dc-link voltage and v_{nN} is the load neutral voltage.

By applying Kirchhoff's laws to Fig. 1, the load voltage and current vectors can be written as

$$\mathbf{v_o} = R_f \mathbf{i} + L_f \frac{di}{dt} + \mathbf{v} - R_n i_n - L_n \frac{di_n}{dt} \tag{11}$$

$$\mathbf{i} = \mathbf{i_o} + C_f \frac{d\mathbf{v_o}}{dt} \tag{12}$$

$$i_n = -(i_a + i_b + i_c)$$

$$i_{on} = -(i_{\rm oa} + i_{\rm ob} + i_{\rm oc}). \tag{13}$$

By solving (11)–(13), the state-space model of the inductive and capacitive filter is computed by

$$\frac{d}{dt}\begin{bmatrix} \mathbf{v_o} \\ \mathbf{i} \end{bmatrix} = \mathbf{A}\begin{bmatrix} \mathbf{v_o} \\ \mathbf{i} \end{bmatrix} + \mathbf{B}\begin{bmatrix} \mathbf{v} \\ \mathbf{i}_o \end{bmatrix} \tag{14}$$

$$\mathbf{A} = \begin{bmatrix} \mathbf{0} & \dfrac{\mathbf{I}}{C_f} \\ -\dfrac{1}{L_{\rm eq}} & -\dfrac{R_{\rm eq}}{L_{\rm eq}} \end{bmatrix}_{6x6} \qquad \mathbf{B} = \begin{bmatrix} \mathbf{0} & \dfrac{-\mathbf{I}}{C_f} \\ -\dfrac{1}{L_{\rm eq}} & \mathbf{0} \end{bmatrix}_{6\times 6}$$

$$R_{\rm eq} = \begin{bmatrix} R_f + R_n & R_n & R_n \\ R_n & R_f + R_n & R_n \\ R_n & R_n & R_f + R_n \end{bmatrix}$$

$$L_{\rm eq} = \begin{bmatrix} L_f + L_n & L_n & L_n \\ L_n & L_f + L_n & L_n \\ L_n & L_n & L_f + L_n \end{bmatrix} \tag{15}$$

where $\mathbf{0}$ and $\mathbf{I}$ are the third-order null and identity matrices, respectively [33].

III. Model-Predictive Control of the qZS Four-Leg Inverter

The block diagram of the proposed predictive-based control approach is shown in Fig. 3. By using the FCS-MPC approach, the cost function can easily manage a multiobjective problem

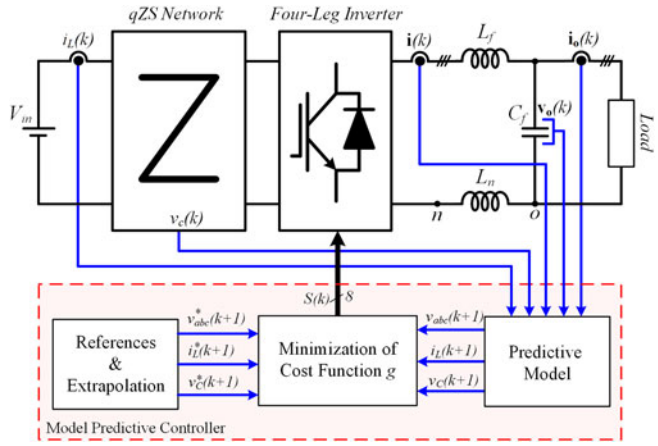

Fig. 3. Proposed FCS-MPC scheme for a qZS four-leg inverter.

and handle the system constraints. The proposed intuitive predictive approach consists of the following four main steps.

A. References and Extrapolation

The output voltage magnitude and frequency are selected to 110 V rms and 50 Hz, respectively. The dc-link voltage reference value is normally obtained through the MPPT algorithm. However, the reference dc-link voltage is selected manually without loss of the main aim of the study. Furthermore, the reference input (inductor) current should be obtained from the inverter power rating. $i_L^* = P/V_{\text{in}}$, where V_{in} and P are the input voltage and power rate of the qZSI, respectively.

Once the references are obtained in the kth instant, they must be extrapolated to the (k+1)th instant for the use within the cost function. When the sampling time T_s is sufficiently small (< 20 μs), no extrapolation is required [34]. In this case, $x^*(k+1) = x^*(k)$. When the sampling time T_s is greater than 20 μs, the following fourth-order Lagrange extrapolation can be used [34]:

$$x^*(k+1) = 4x^*(k) - 6x^*(k-1) + 4x^*(k-2) - x^*(k-3). \quad (16)$$

B. Predictive Models

The digital implementation of the proposed control algorithm requires a discrete-time model of the control parameters. Since the proposed controller handles three control objectives, the predictive model of the system requires three discrete-time equations. This paper considers a first-order approximation (17) for the derivative computation due to the first-order nature of the state equations

$$\frac{dx}{dt} = \frac{x(k) - x(k-1)}{T_s}. \quad (17)$$

1) Predictive Model I: To predict the future behavior of the output voltage vector ($\mathbf{v_o}$), the mathematical model of the four-leg inverter, which is given in Section II, is employed. The continuous-time expression for the $\mathbf{v_o}$ is given in (14). By substituting (17) into (14), the discrete-time model can be obtained as

$$\begin{bmatrix} \mathbf{v_o}(k+1) \\ \mathbf{i}(k+1) \end{bmatrix} = \Phi \begin{bmatrix} \mathbf{v_o}(k) \\ \mathbf{i}(k) \end{bmatrix} + \Gamma \begin{bmatrix} \mathbf{v}(k) \\ \mathbf{i_o}(k) \end{bmatrix}$$
$$\Phi = e^{\mathbf{A}Ts}\Gamma = \mathbf{A}^{-1}(\Phi - \mathbf{I}_{6\times 6})\mathbf{B}. \quad (18)$$

2) Predictive Model II: To predict future behavior of the inductor current (i_L), the inductor voltage model is employed. The continuous-time model of the inductor voltage can be expressed as

$$v_{L1} = L\frac{di_L}{dt} \quad (19)$$

where L is the inductance of the inductor. Based on (19), the inductor current is derived as

$$\frac{di_L}{dt} = \frac{1}{L}v_L. \quad (20)$$

By substituting (17) into (20), the discrete-time model of the i_L can be obtained as

$$i_L(k+1) = i_L(k) + \frac{T_s}{L}v_L(k) \quad (21)$$

where $i_L(k+1)$ is the predicted inductor current at the next sampling time, and $v_L(k)$ is the inductor voltage that depends on the states of the qZS topology. According to the operational principle of the qZS network that was explained in Section II, for the nonshoot-through and the shoot-through states, inductor voltage can be defined as follows.

1) During nonshoot-through state:

$$v_L = V_{\text{in}} - v_{C1}. \quad (22)$$

2) During shoot-through state:

$$v_L = V_{\text{in}} + v_{C2}. \quad (23)$$

3) Predictive Model III: This model is employed to predict future behavior of the capacitor voltage (V_{C1}). The continuous-time model of the capacitor current can be expressed as

$$i_{C1} = C_1\frac{dv_{C1}}{dt} \quad (24)$$

where C_1 is the capacitance of the capacitor. Based on (24), the capacitor voltage is derived as

$$\frac{dv_{C1}}{dt} = \frac{1}{C_1}i_{C1}. \quad (25)$$

By substituting (17) into (25), the discrete-time model of the v_{C1} can be obtained as

$$v_{C1}(k+1) = v_{C1}(k) + \frac{T_s}{C}i_{C1}(k) \quad (26)$$

where $v_{C1}(k+1)$ is the predicted capacitor voltage at the next sampling time, and $i_{C1}(k)$ is the capacitor current that depends on the states of the qZSI topology. For the nonshoot-through and the shoot-through states, capacitor current can be defined as follows.

1) During nonshoot-through state:

$$i_{C1} = i_{L1} - (S_a i_a + S_b i_b + S_c i_c). \quad (27)$$

2) During shoot-through state:

$$i_{C1} = -i_{L1}. \tag{28}$$

C. Minimization of the Cost Function

To handle the desired control objectives, three cost functions are defined. The first term in the cost function is responsible to minimize the error between the reference and predicted voltage vectors

$$g_{v_o}(k+1) = \|\mathbf{v}_\mathbf{o}^*(k+1) - \mathbf{v}_\mathbf{o}(k+1)\|^2 \tag{29}$$

where $\mathbf{v}_\mathbf{o}^*(k+1)$ is the reference output voltage vector and $\mathbf{v}_\mathbf{o}(k+1)$ is the predicted output voltage vector in the next step. The second term of the cost function handles the reference tracking of inductor current, which is defined as

$$g_{I_L}(k+1) = |i_L^*(k+1) - i_L(k+1)| \tag{30}$$

where $i_L^*(k+1)$ and $i_L(k+1)$ are the reference and predicted inductor currents in the next step, respectively. The last term of the cost function minimizes the error between the reference and predicted capacitor voltage values

$$g_{v_C}(k+1) = |v_{C1}^*(k+1) - v_{C1}(k+1)| \tag{31}$$

where $v_{C1}^*(k+1)$ and $v_{C1}(k+1)$ are the reference and predicted capacitor voltages in the next step, respectively. The complete cost function is

$$g(k+1) = g_{v_o}(k+1) + \lambda_i.g_{i_L}(k+1) + \lambda_v.g_{v_C}(k+1) \tag{32}$$

where λ_i and λ_v are the weighting factors. Tuning of these factors will be discussed in Section IV-A.

D. Control Algorithm

Fig. 4 shows the FCS-MPC-based control algorithm in the flowchart form. As shown in Fig. 4, predictive models II and III depend on the switching states, while the predictive model is independent from the switching states. To select correct predictive models, a simple detection algorithm is employed in a very simple way: If $k \leqslant 15$, then the state is nonshoot-through, and if $k = 16$, the state is shoot-through state. The switching states of the inverter are given in Table I. The corresponding switching state is selected by the cost function, which stores the minimum error.

IV. Simulation and Experimental Results

Simulations and experiments are carried out to show the performance and effectiveness of the proposed FCS-MPC in controlling the qZS four-leg inverter. The proposed control algorithm has been implemented in a dSPACE DS1006 controller board. The currents and voltages are measured by LEM LA 100-P and LV 25-P transducers, respectively. The inverter prototype has been built by Semikron SKM75GB12T4 dual insulated-gate bipolar transistor modules. The parameters used in the simulation and experimental tests are the same, and they are summarized in Table II.

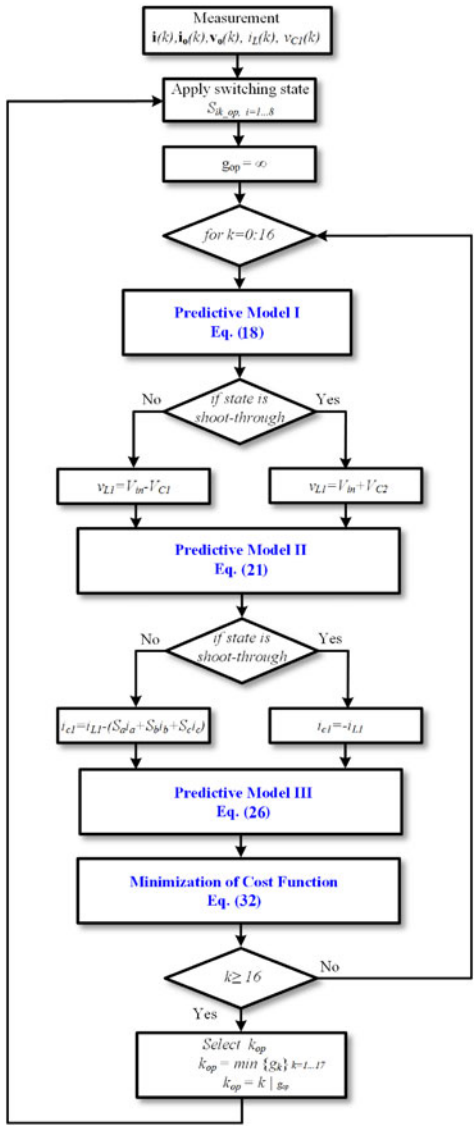

Fig. 4. Flowchart of the proposed FCS-MPC algorithm.

TABLE II
qZS Four-Leg Inverter and Load Parameters

Parameter	Value
Input dc voltage (V_{in})	150 V
qZS network inductances (L_1, L_2)	1.0 mH
qZS network capacitances (C_1, C_2)	1000 μF
Filter inductance, (L_f, L_n)	5 mH
Filter resistance (R_f, R_n)	0.02 Ω
Filter capacitance (C_f)	40 μF
Nominal load voltage (v_o^*)	110 V rms
Nominal frequency (f_o)	50 Hz
Sampling time (T_s)	50 μs

A. Tuning of Weighting Factors

Since the proposed FCS-MPC technique is based on the multioptimization problem, the weighting factors (λ_i and λ_v) are first tuned to guarantee the stability and desired performance of the system. However, the weighting factor selection is still an

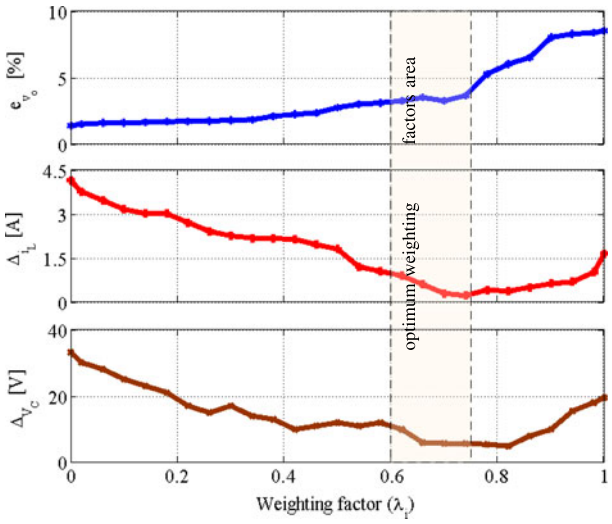

Fig. 5. Weighting factor influence on the output voltage, the input current, and the capacitor voltage.

open topic for research. Right now, there are no analytical or numerical methods to adjust weighting factors, which are determined based on empirical procedures. In this study, the tuning is conducted based on minimizing the error on the output voltage ($e_{\rm vo}$) and minimizing the double-line frequency ($2f_o$) ripple on the input current ($\triangle_{i_{L1}}$) and the capacitor voltage ($\triangle_{V_{C2}}$). To observe the effect of λ_i and λ_v on the performance and selecting the optimum value for the best control results, $e_{\rm vo}$, $\triangle_{i_{L1}}$, and $\triangle_{V_{C2}}$ (these variables are selected as performance indicators for the selection of the optimum weighting factors) were measured for different values of λ_i and λ_v. To simplify the analysis, λ_v is chosen equal to 0.1*λ_i. To observe the effect of the $2f_o$ on i_{L1} and V_{C2}, this test was performed with unbalanced load condition. Fig. 5 shows the variation of $e_{\rm vo}$, $\triangle_{i_{L1}}$, and $\triangle_{V_{C2}}$ as a function of λ_i. The results have been obtained by performing several simulations, starting with $\lambda_i = 0$ and gradually increasing these values. It can be observed (see Fig. 5) that a reduction of the ripples on the inductor current and the capacitor voltages introduces higher reference tracking error on the output voltage, which affects the quality of the output current as well. This tradeoff is very clear in Fig. 5. Notice that the optimum performance is obtained for λ_i between 0.6 and 0.75 since the voltage error is still below 5% of the rated voltage and a significantly reduction is achieved for the inductor current and the capacitor voltage ripples. Thus, $\lambda_i = 0.75$ and $\lambda_v = 0.075$ are considered as the optimum weighting factors and are used for the simulation and experimental tests.

B. Steady-State Analysis

To test steady-state performance of the proposed system, the following four cases are considered. For all cases, the input voltage is $V_{\rm in} = 150$ V and the reference capacitor voltage is $V_{c1}^* = 225$ V. The load topologies used in the experiments are shown in Fig. 6.

(1) *Case C1:* balanced reference voltages ($v_{\rm oa}^* = v_{\rm ob}^* = v_{oc}^* = 110$ V) and balanced loads (R_a=R_b=R_c=10 Ω) [see Fig. 6(a)].

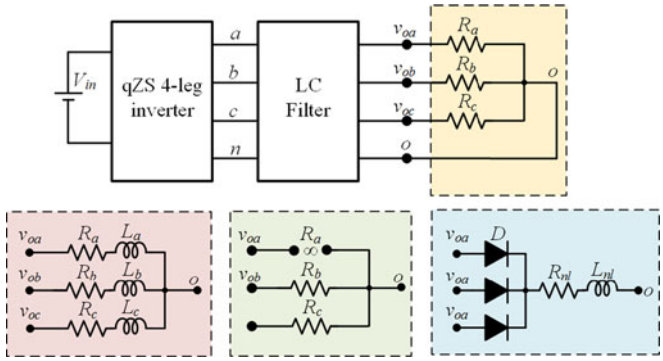

Fig. 6. Load topologies used in the simulations and experiments. (a) R load. (b) RL load. (c) One-phase open R load. (d) Half-bridge rectifier with RL load.

(2) *Case C2:* balanced reference voltages ($v_{\rm oa}^* = v_{\rm ob}^* = v_{oc}^* = 110$ V) and single-phase RL loads ($R_a = 30\,\Omega$, $R_b = 10\,\Omega$, $R_c = 6\,\Omega$, $L_a = 0$ mH, $L_b = 5$ mH, $L_c = 5$ mH) [see Fig. 6(b)].

(3) *Case C3:* balanced reference voltages ($v_{\rm oa}^* = v_{\rm ob}^* = v_{oc}^* = 110$ V) and single-phase no loads ($R_a = \infty\ \Omega$, $R_b = R_c = 10\ \Omega$) [see Fig. 6(c)].

(4) *Case C4:* balanced reference voltages ($v_{\rm oa}^* = v_{\rm ob}^* = v_{oc}^* = 110$ V) and a combination of balanced ($R_a = R_b = R_c = 10\ \Omega$) [see Fig. 6(a)] and RL load as shown in Fig. 6(d) ($R_{nl} = 10\ \Omega$, $L_{nl} = 10$ mH).

Fig. 7(a)–(d) shows the steady-state performance of the proposed system. It can be seen that the output voltages ($v_{\rm oa}, v_{\rm ob}, v_{oc}$), the inductor current (i_{L1}), and the capacitor voltage (V_{C1}) track their references with high accuracy for all cases. It is shown that the dc-link voltage is 300 V, which confirms theoretical analysis in Section II. It is also clear that the neutral current (i_n) is zero for cases C1 and C4 [see Fig. 7(a) and (d)]. The neutral current, however, appears in the fourth leg for cases C2 and C3 [see Fig. 7(b) and (c)].

C. Transient-State Analysis

1) *Case D1:* balanced reference voltages ($v_{\rm oa}^* = v_{\rm ob}^* = v_{oc}^* = 110$ V). A step change from balanced loads ($R_a = R_b = R_c = 30\ \Omega$) to balanced loads ($R_a = R_b = R_c = 15\ \Omega$).

2) *Case D2:* balanced reference voltages ($v_{\rm oa}^* = v_{\rm ob}^* = v_{oc}^* = 110$ V). A step change from balanced loads ($R_a = R_b = R_c = 15\ \Omega$) to unbalanced loads ($R_a = 15\ \Omega$, $R_b = 30\ \Omega$, $R_c = 22.5\ \Omega$).

3) *Case D3:* balanced reference voltages ($v_{\rm oa}^* = v_{\rm ob}^* = v_{oc}^* = 110$ V). A step change from balanced loads ($R_a = R_b = R_c = 15\ \Omega$) to no load in Phase b ($R_a = R_c = 15\ \Omega$, $R_b = \infty\ \Omega$).

4) *Case D4:* balanced reference voltages ($v_{\rm oa}^* = v_{\rm ob}^* = v_{oc}^* = 110$ V). A step change from balanced loads ($R_a = R_b = R_c = 15\ \Omega$) to no load in Phase b and c ($R_a = 15\ \Omega$, $R_b = R_c = \infty\ \Omega$).

The results of the first and second cases are depicted in Fig. 8(a) and (b). It can be seen that transient response is very fast, and no overshot is observed. Furthermore, the disturbance

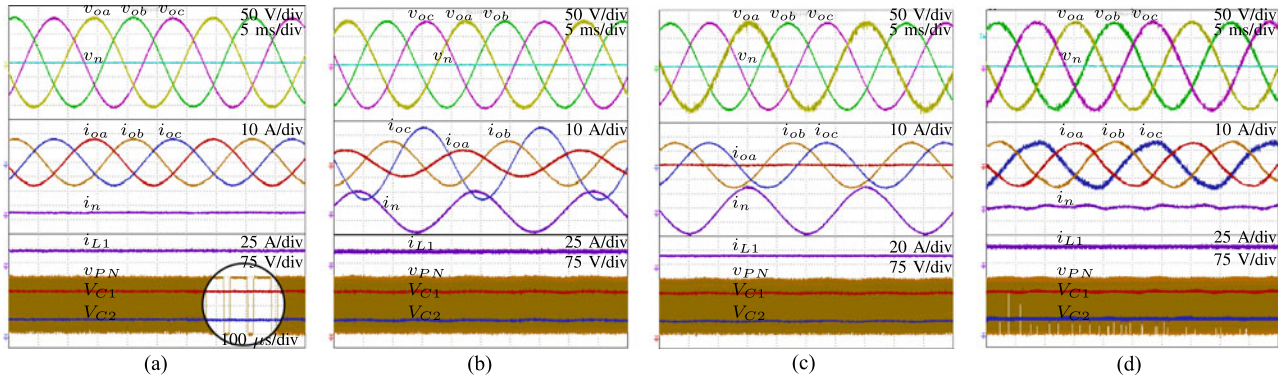

Fig. 7. Experimental results of the steady-state analysis with (a) balanced resistive loads, (b) unbalanced single-phase RL loads, (c) single-phase no load, and (d) combination of balanced R and RL loads.

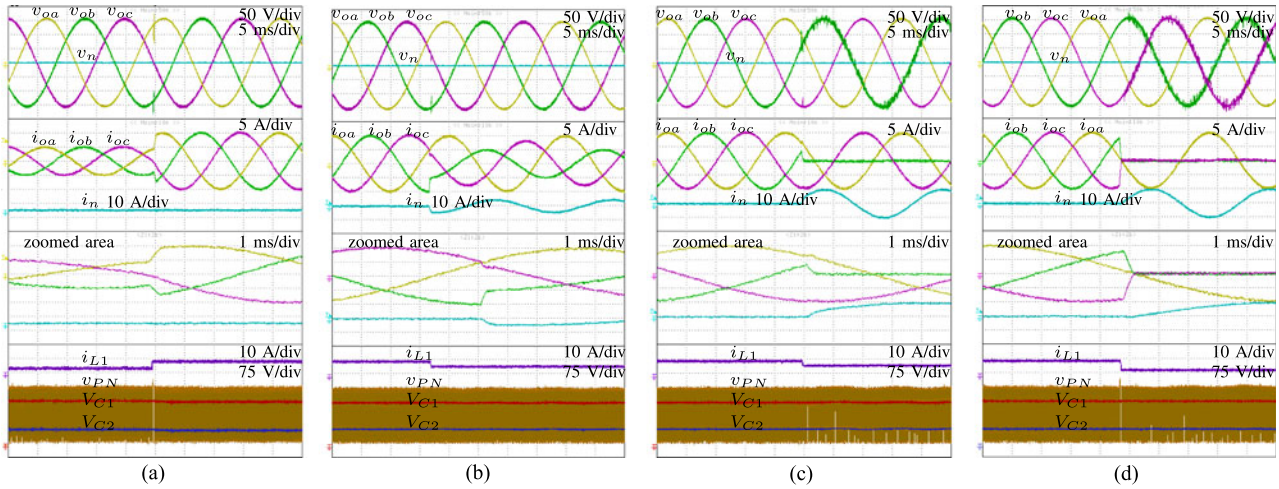

Fig. 8. Experimental results of the transient-state analysis with (a) balanced reference voltages and balanced load step, (b) balanced reference voltages and unbalanced load step, (c) balanced reference voltages and no load in phase b, and (d) balanced reference voltages and no load in phases b and c.

in the load voltage is very small, and it can be neglected at load change step. Note that the neutral current (i_n) appears under the unbalanced load condition [see Fig. 8(b)].

The proposed system is also tested under one-phase and two-phase open circuit conditions, which may occur during the operation of such power converters in islanding mode (cases D3 and D4). This is investigated because single-phase and two-phase loads are common in islanding operation. The experimental results of one-phase and two-phase open-circuit conditions are given in Fig. 8(c) and (d), respectively. From these cases, it is evident that the controller is very robust and reliable, withstanding the one-phase and two-phase open-circuit conditions. It is remarkable to note that there is no significant disturbance on the qZS network voltage ($V_{\rm PN}$) and current (i_{L1}) under these tests.

D. Robustness to Parameters Variations Analysis

Since the proposed controller is model based, the accuracy of the controller depends on the system parameters. For this reason, the objective of this section is to investigate the robustness of the proposed predictive control to the parameters variations of the filter and qZS network inductances and capacitances. It is worth to mention that during the study, the controller is unaware of the parameters variations and remains using the rated parameters given in Table II. The parameter variations have been analyzed through simulations. During the simulations, balanced reference voltages ($v^*_{\rm oa} = v^*_{\rm ob} = v^*_{\rm oc}$=110 V rms) and unbalanced loads ($R_a = 10\ \Omega$, $R_b = 5\ \Omega$, $R_c = 5\ \Omega$) are considered.

To show filter parameter effect on the system performance, the percentage mean absolute voltage reference tracking error (%e) and total percentage harmonic distortion (THD) are calculated according to the guidelines given in [35]. Furthermore, to observe the qZS source network parameter effect on the controller, the ripples on the capacitor voltage (Δ_{V_c}) and the inductor current (Δ_{i_L}) are calculated. The obtained simulation results are shown in Fig. 9(a)–(d). It can be noted that these variations have little impact on the %THD, $\%e_{v_o}$, Δ_{i_L}, and Δ_{V_C}. The variations in C_f have more impact on the $\%e_{v_o}$ than the L_f variations. In addition, it can be observed that minimum Δ_{i_L} and Δ_{V_C} are ensured at the rated value of the qZS source network's inductance and capacitance, respectively. In conclusion, even with the mismatch filter and qZS network parameters, the proposed FCS-MPC can handle this issue without significant impact on the system performance and shows that relatively low sensitive to parameters change.

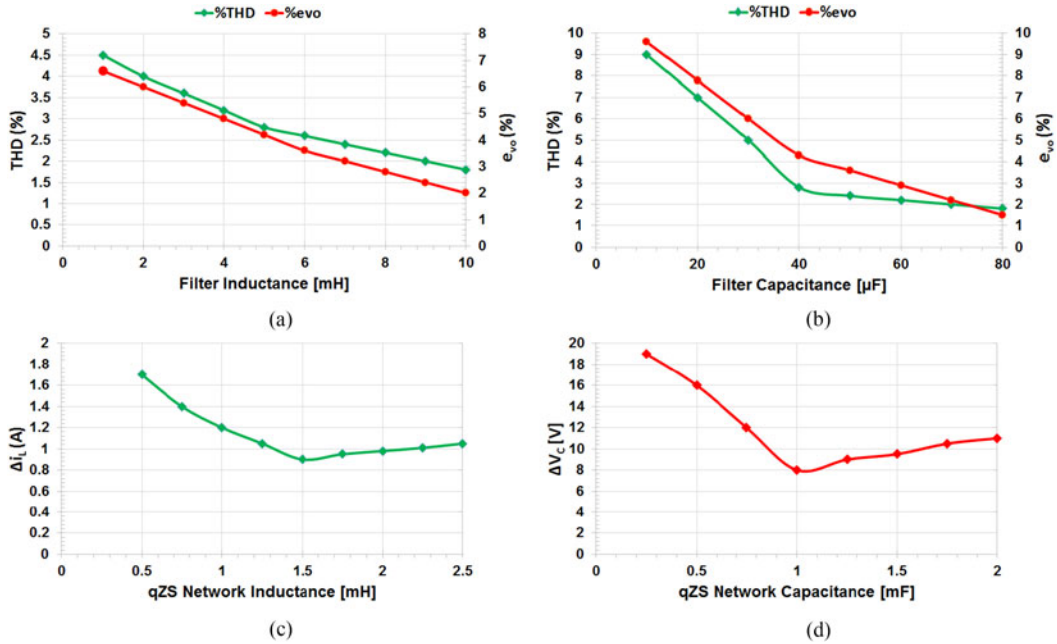

Fig. 9. Simulation results of the robustness analysis with parameter variations. (a) Changes to filter inductance (L_f). (b) Changes to filter capacitance (L_f). (c) Changes to qZS network inductances (L_1 and L_2). (d) Changes to qZS network capacitances (C_1 and C_2).

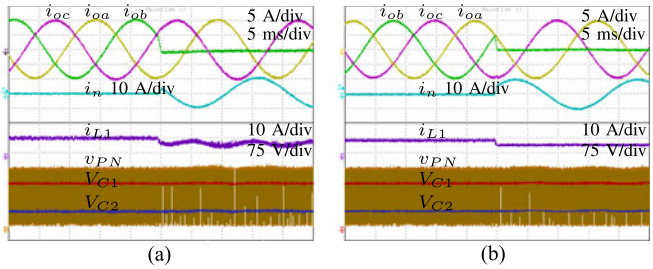

Fig. 10. Performance comparison under unbalanced load (a) with two cost functions and (b) with three cost functions.

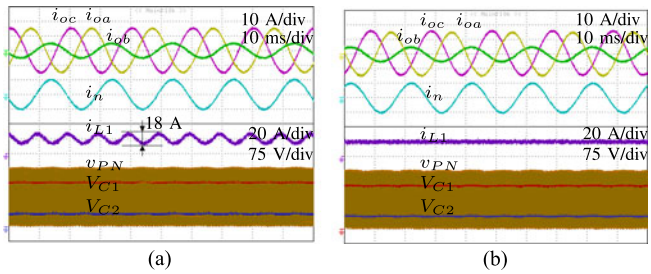

Fig. 11. Experimental results of qZS four-leg inverter with (a) two cost functions and (b) three cost functions.

E. Analysis of DC-Side Low-Frequency Power

To overcome $2f_o$ ripple in the inductor current, the third term (g_{i_L}) is added in the cost function. To verify the effect of g_i on the control performance, the proposed four-leg inverter is also tested with two terms in the cost function, which are g_{vo} and g_{vc}. The obtained experimental results of this test are shown in Fig. 10(a) and (b). At the beginning of this test, the output loads were balanced. The double-line frequency has appeared neither in the inductor current nor in the capacitor voltage for both control algorithms (two or three terms in the cost functions). Then, the load connected to "phase b" was disconnected from the inverter in order to generate unbalanced current. After such an action, an unbalanced current flowed through the fourth leg of the inverter [see Fig. 10(a) and (b)]. In Fig. 10(a), during the unbalanced situation, the $2f_o$ ripple appeared in the inductor current, while the $2f_o$ ripple was eliminated in Fig. 10(b) by integrating the third term in the cost function. It is concluded that the FCS-MPC algorithm, which has three terms in the cost function, shows much better performance under unbalance load situation. However, it can be observed from Fig. 10(b) that $2f_o$ ripple still exists on the capacitor and dc-link voltages. These ripples are very low and can be tolerated by the capacitors.

The existing FCS-MPC (two terms in the cost function) algorithm and the proposed FCS-MPC algorithm also affect the design and cost of the qZS four-leg inverter. Experimental results of Fig. 11(a) and (b) correspond to the cases without and with the third term in the cost function, respectively. Both algorithms are tested with the same inverter parameters, which are given in Table II. From Fig. 11(a), it is evident that the qZS inductor has 18-A peak-to-peak $2f_o$ ripple current. On the other hand, it can be seen from Fig. 11(b) that $2f_o$ ripple current is eliminated when the third term is integrated in the cost function.

To observe the effect of the $2f_o$ ripple on the inverter parameters, cost analysis was also done. As mentioned above, one way to minimize $2f_o$ ripple in the inductor current is to use large qZS source inductance. For comparison purpose, to reduce $2f_o$ ripple of the inductor current from 18 to 4 A without the third term in the cost function, the inductor parameter was designed by using the guidelines given in [36]. Table III summarizes the used in this paper (1 mH) and the designed earlier inductances (5 mH) in terms of price, dimensions, and weight. It is noticeable that the price, weight, and dimensions of earlier designed inductance are much higher than the used one according to the proposed approach. The price difference of two inductances is

TABLE III
COMPARISON OF USED AND NEW DESIGN INDUCTANCES

	Used Parameter	Designed Parameter
Value	1 mH/30 A	5 mH/30 A
Price [USD]	120 × 2=240	299 × 2=598
Weight [kg]	2.60	7.28
Dimensions [in]	3.75 × 3.85 ×3.13	5.25 × 5.0 × 4.47

Note: Data are from Mouser website. Manufacturer part numbers of 1 mH and 5 mH inductances are 195C30 and 195G30. The brand of the inductances is Hammond manufacturing.

358 USD. Furthermore, the weight of designed inductance is almost three times higher than the used one. In conclusion, adding one extra term in the cost function eliminates $2f_o$ ripple in the inductor current, which brings considerable benefits in terms of the size, weight, and overall inverter cost.

V. CONCLUSION

This paper presented the FCS-MPC approach for three-phase qZS four-leg inverter under unbalanced load condition. Similar to the single-phase inverter, double-line frequency ($2f_o$) ripple appeared in the dc-link voltage and current in the case of unbalanced load condition. This $2f_o$ ripple led to reduce the overall system performance in terms of efficiency. To overcome this problem with effective and simple way, the FCS-MPC-based control algorithm was employed. This algorithm was entirely based on the discrete-time model of the system. The behavior of the predictive controller was investigated, and the changes to both the qZS network and filter inductive and capacitor parameters were considered. Furthermore, the weighting factor tuning was conducted based on minimizing the error on the output voltage (e_{vo}) and minimizing the double-line frequency ($2f_o$) ripple on the input current ($\triangle_{i_{L1}}$) and the capacitor voltage ($\triangle_{V_{C2}}$).

To verify the performance of the proposed approach, simulation and experimental studies were performed with the single/three-phase and balanced/unbalanced loads. Through the simulation and experimental results, it was demonstrated that the proposed control approach offers a powerful technique for the control of the qZS four-leg inverter under unbalanced load condition.

ACKNOWLEDGMENT

This publication was made possible by NPRP-EP X-033-2-007 (Sections I and II) and NPRP 8-241-2-095 (Sections III, IV, and V) from the Qatar National Research Fund (a member of Qatar Foundation). The statements made herein are solely the responsibility of the authors.

REFERENCES

[1] J. G. de Matos, F. S. F. eSilva, and L. A. d. S. Ribeiro, "Power control in ac isolated microgrids with renewable energy sources and energy storage systems," *IEEE Trans. Ind. Electron.*, vol. 62, no. 6, pp. 3490–3498, Jun. 2015.

[2] H. Abu-Rub, M. Malinowski, and K. Al-Haddad, *Power Electronics for Renewable Energy Systems, Transportation and Industrial Applications*. Hoboken, NJ, USA: Wiley, 2014.

[3] S. Kouro, J. Leon, D. Vinnikov, and L. Franquelo, "Grid-connected photovoltaic systems: An overview of recent research and emerging PV converter technology," *IEEE Ind. Electron. Mag.*, vol. 9, no. 1, pp. 47–61, Mar. 2015.

[4] M. Malinowski, A. Milczarek, R. Kot, Z. Goryca, and J. T. Szuster, "Optimized energy-conversion systems for small wind turbines: Renewable energy sources in modern distributed power generation systems," *IEEE Power Electron. Mag.*, vol. 2, no. 3, pp. 16–30, Sep. 2015.

[5] O. Ellabban, H. Abu-Rub, and S. Bayhan, "Z-source matrix converter: An overview," *IEEE Trans. Power Electron.*, vol. 31, no. 11, pp. 7436–7450, Nov. 2015.

[6] D. Sun, B. Ge, W. Liang, H. Abu-Rub, and F. Z. Peng, "An energy stored quasi-z-source cascade multilevel inverter-based photovoltaic power generation system," *IEEE Trans. Ind. Electron.*, vol. 62, no. 9, pp. 5458–5467, Sep. 2015.

[7] S. Bayhan, M. Trabelsi, and H. Abu-Rub, "Model predictive control of three-phase three-level neutral-point-clamped qZS inverter," in *Proc. 10th Int. Conf. Compat. Power Electron. Power Eng.*, Jun. 2016, pp. 410–415.

[8] O. Ellabban and H. Abu-Rub, "Z-source inverter: Topology improvements review," *IEEE Ind. Electron. Mag.*, vol. 10, no. 1, pp. 6–24, Spring 2016.

[9] G.-H. Kim, C. Hwang, J.-H. Jeon, J.-B. Ahn, and E.-S. Kim, "A novel three-phase four-leg inverter based load unbalance compensator for standalone microgrid," *Int. J. Elect. Power Energy Syst.*, vol. 65, pp. 70–75, Feb. 2015.

[10] X. Li, Z. Deng, Z. Chen, and Q. Fei, "Analysis and simplification of three-dimensional space vector PWM for three-phase four-leg inverters," *IEEE Trans. Ind. Electron.*, vol. 58, no. 2, pp. 450–464, Feb. 2011.

[11] M. Sedlak, S. Stynski, M. P. Kazmierkowski, and M. Malinowski, "Operation of four-leg three-level flying capacitor grid-connected converter for res," in *Proc. 39th Annu. Conf. IEEE Ind. Electron. Soc.*, Nov. 2013, pp. 1100–1105.

[12] S. Bayhan and H. Abu-Rub, *Impedance Source Multi-Leg Inverters*. Hoboken, NJ, USA: Wiley, 2016, pp. 295–328. [Online]. Available: http://dx.doi.org/10.1002/9781119037088.ch17

[13] M. Dai, M. N. Marwali, J. W. Jung, and A. Keyhani, "A three-phase four-wire inverter control technique for a single distributed generation unit in island mode," *IEEE Trans. Power Electron.*, vol. 23, no. 1, pp. 322–331, Jan. 2008.

[14] E. Demirkutlu and A. Hava, "A scalar resonant-filter-bank-based output-voltage control method and a scalar minimum-switching-loss discontinuous PWM method for the four-leg-inverter-based three-phase four-wire power supply," *IEEE Trans. Ind. Appl.*, vol. 45, no. 3, pp. 982–991, May/Jun. 2009.

[15] S. B. Karanki, N. Geddada, M. K. Mishra, and B. K. Kumar, "A modified three-phase four-wire UPQC topology with reduced dc-link voltage rating," *IEEE Trans. Ind. Electron.*, vol. 60, no. 9, pp. 3555–3566, Sep. 2013.

[16] M. R. Miveh, M. F. Rahmat, A. A. Ghadimi, and M. W. Mustafa, "Control techniques for three-phase four-leg voltage source inverters in autonomous microgrids: A review," *Renew. Sustain. Energy Rev.*, vol. 54, pp. 1592–1610, Feb. 2016.

[17] S. Bifaretti, A. Lidozzi, L. Solero, and F. Crescimbini, "Comparison of modulation techniques for active split dc-bus three-phase four-leg inverters," in *Proc. IEEE Energy Convers. Congr. Expo.*, Sep. 2014, pp. 5631–5638.

[18] Z. Min, "Investigation of switching schemes for three-phase four-leg voltage source inverters," Ph.D. dissertation, School Electr. Electron. Eng., Newcastle Univ., Newcastle, U.K., Jun. 2013.

[19] M. Trabelsi, K. A. Ghazi, N. Al-Emadi, and L. Ben-Brahim, "An original controller design for a grid connected PV system," in *Proc. 38th Annu. Conf. IEEE Ind. Electron. Soc.*, Oct. 2012, pp. 924–929.

[20] M. Trabelsi, L. Ben-Brahim, and K. A. Ghazi, "An improved real-time digital feedback control for grid-tie multilevel inverter," in *Proc. 39th Annu. Conf. IEEE Ind. Electron. Soc.*, Nov. 2013, pp. 5776–5781.

[21] D. Patel, R. Sawant, and M. Chandorkar, "Three-dimensional flux vector modulation of four-leg sine-wave output inverters," *IEEE Trans. Ind. Electron.*, vol. 57, no. 4, pp. 1261–1269, Apr. 2010.

[22] Y. Liu, B. Ge, H. Abu-Rub, and F. Z. Peng, "Overview of space vector modulations for three-phase z-source/quasi-z-source inverters," *IEEE Trans. Power Electron.*, vol. 29, no. 4, pp. 2098–2108, Apr. 2014.

[23] S. Vazquez, A. Marquez, R. Aguilera, D. Quevedo, J. I. Leon, and L. G. Franquelo, "Predictive optimal switching sequence direct power control for grid-connected power converters," *IEEE Trans. Ind. Electron.*, vol. 62, no. 4, pp. 2010–2020, Apr. 2015.

[24] S. Bayhan, M. Mosa, and H. Abu-Rub, *Model Predictive Control of Impedance Source Inverter*. Hoboken, NJ, USA: Wiley, 2016, pp. 329–361. [Online]. Available: http://dx.doi.org/10.1002/9781119037088.ch18
[25] H. Young, M. Perez, J. Rodriguez, and H. Abu-Rub, "Assessing finite-control-set model predictive control: A comparison with a linear current controller in two-level voltage source inverters," *IEEE Ind. Electron. Mag.*, vol. 8, no. 1, pp. 44–52, Mar. 2014.
[26] D.-K. Choi and K.-B. Lee, "Dynamic performance improvement of ac/dc converter using model predictive direct power control with finite control set," *IEEE Trans. Ind. Electron.*, vol. 62, no. 2, pp. 757–767, Feb. 2015.
[27] M. Trabelsi, S. Bayhan, K. Ghazi, H. Abu-Rub, and L. Ben-Brahim, "Finite control set model predictive control for grid connected packed-U-cells multilevel inverter," *IEEE Trans. Ind. Electron.*, vol. 63, no. 11, pp. 7286–7295, Nov. 2016.
[28] S. Bayhan, H. Abu-Rub, and R. S. Balog, "Model predictive control of quasi-z-source four-leg inverter," *IEEE Trans. Ind. Electron.*, vol. 63, no. 7, pp. 4506–4516, Jul. 2016.
[29] M. Narimani, B. Wu, V. Yaramasu, Z. Cheng, and N. Zargari, "Finite control-set model predictive control (FCS-MPC) of nested neutral point clamped (NNPC) converter," *IEEE Trans. Power Electron.*, vol. 30, no. 12, pp. 7262–7269, Dec. 2015.
[30] A. Calle-Prado, S. Alepuz, J. Bordonau, J. Nicolas-Apruzzese, P. Cortés, and J. Rodriguez, "Model predictive current control of grid-connected neutral-point-clamped converters to meet low-voltage ride-through requirements," *IEEE Trans. Ind. Electron.*, vol. 62, no. 3, pp. 1503–1514, Mar. 2015.
[31] L. Ben-Brahim, A. Gastli, M. Trabelsi, K. Ghazi, M. Houchati, and H. Abu-Rub, "Modular multilevel converter circulating current reduction using model predictive control," *IEEE Trans. Ind. Electron.*, vol. 63, no. 6, pp. 3857–3866, Jun. 2016.
[32] S. Bayhan and H. Abu-Rub, "Model predictive control of quasi-z source three-phase four-leg inverter," in *Proc. 41st Annu. Conf. IEEE Ind. Electron. Soc.*, 2015, pp. 362–367.
[33] V. Yaramasu, M. Rivera, M. Narimani, B. Wu, and J. Rodriguez, "Model predictive approach for a simple and effective load voltage control of four-leg inverter with an output *LC* filter," *IEEE Trans. Ind. Electron.*, vol. 61, no. 10, pp. 5259–5270, Oct. 2014.
[34] M. Rivera, V. Yaramasu, A. Llor, J. Rodriguez, B. Wu, and M. Fadel, "Digital predictive current control of a three-phase four-leg inverter," *IEEE Trans. Ind. Electron.*, vol. 60, no. 11, pp. 4903–4912, Nov. 2013.
[35] V. Yaramasu, M. Rivera, B. Wu, and J. Rodriguez, "Model predictive current control of two-level four-leg inverters—Part I: Concept, algorithm, and simulation analysis," *IEEE Trans. Power Electron.*, vol. 28, no. 7, pp. 3459–3468, Jul. 2013.
[36] B. Ge *et al.*, "Current ripple damping control to minimize impedance network for single-phase quasi-z source inverter system," *IEEE Trans. Ind. Informat.*, vol. 12, no. 3, pp. 1043–1054, Jun. 2016.

Sertac Bayhan (M'14) received the B.Sc. (as valedictorian), M.Sc., and Ph.D. degrees from Gazi University, Ankara, Turkey, in 2006, 2008, and 2012, respectively, all in electrical engineering.

He has been a Faculty Member with the Department of Electronic and Automation, Gazi University, since 2009. He is also currently an Assistant Research Scientist with Texas A&M University at Qatar, Doha, Qatar. He has authored more than 60 high-impact journal and conference papers. He is the coauthor of one book and two book chapters. His research interests include power electronics, renewable energy conversion for photovoltaic and wind systems, condition monitoring and power quality detection in power systems, microgrid, and smart grid applications.

Dr. Bayhan has received many prestigious national and international awards, such as the Texas A&M University at Qatar Research Fellow Excellence Award in 2016, the Best Presentation Recognition at the 41st Annual Conference of the IEEE Industrial Electronics Society in 2015, Research Excellence Travel Awards in 2014 and 2015 (at Texas A&M University at Qatar), and Paper Support Awards in 2009, 2014, 2015, and 2016 (from the Scientific and Technological Research Council of Turkey).

Mohamed Trabelsi (M'10) was born in Tunis, Tunisia, in January 1982. He received the B.Sc. degree in electrical engineering from the National Institute of Applied Science and Technology, Tunis, Tunisia, in 2006, and the M.Sc. degree in automated systems and the Ph.D. degree in energy systems from INSA Lyon, Villeurbanne, France, in 2006 and 2009, respectively.

From October 2009 to November 2013, he was a Postdoctoral Fellow at Qatar University. From December 2013 to November 2014, he was a Postdoctoral Fellow at Texas A&M University at Qatar, Doha, Qatar, where he is currently an Assistant Research Scientist (Assistant Professor for Research). He has published more than 40 journal and conference papers, and he is an author of one book and one book chapter. His research interests include system control with applications arising in the contexts of power electronics, energy conversion, renewable energy, and smart grids. He has been participating as Principal Investigator in several collaborative research projects for the Qatar National Research Fund (QNRF), resulting in more than $6 million of funding in collaborative research over the last three years.

Dr. Trabelsi received the prestigious French MENRT Scholarship from the Ministry of Highest Education for postgraduate studies.

Haitham Abu-Rub (M'99—SM'07) received the M.Sc. degree from the Maritime Academy of Gdynia, Gdynia, Poland, 1990, and the Ph.D. degree from the Technical University of Gdańsk, Gdańsk, Poland, in 1995, both in electrical engineering. He also received another Ph.D. degree in humanities from the University of Gdańsk, in 2004.

Since 2006, he has been with Texas A&M University at Qatar, Doha, Qatar, where he is currently a Professor. He is currently the Chair of the Electrical and Computer Engineering Program, Texas A&M University at Qatar, as well as the Managing Director of the Smart Grid Center Extension. He has authored more than 250 journal and conference papers and has earned and supervised many research projects. He is currently leading many projects on photovoltaic and hybrid renewable power generation systems with different types of converters and on electric drives. He is the coauthor of four books, two of which are published by Wiley. He is also an author or coauthor of five book chapters. His research interests include energy conversion systems, including electric drives, power electronic converters, renewable energy, and smart grid.

Dr. Abu-Rub is an Editor of several IEEE journals. He has received many prestigious international awards, such as the American Fulbright Scholarship, the German Alexander von Humboldt Fellowship, the German DAAD Scholarship, and the British Royal Society Scholarship.

Mariusz Malinowski (S'99–M'03–SM'08–F'13) received the Ph.D. and D.Sc. degrees in electrical engineering from the Institute of Control and Industrial Electronics, Warsaw University of Technology (WUT), Warsaw, Poland, in 2001 and 2012, respectively.

He was a Visiting Scholar at Aalborg University, Aalborg, Denmark; the University of Nevada, Reno, NV, USA; the Technical University of Berlin, Berlin, Germany; and ETH Zurich, Zurich, Switzerland. He is currently with the Institute of Control and Industrial Electronics, WUT. His current research interests include the control and modulation of grid-side converters, multilevel converters, smart grids, and power-generation systems based on renewable energies. He has coauthored more than 130 technical papers and six books. He holds two implemented patents.

Prof. Malinowski received the Siemens Prize in 2002 and 2007, the WUT President Scientific Prize in 2015, the Polish Minister of Science and the Higher Education Awards in 2003 and 2008, respectively, the Prime Minister of Poland Award for Habilitation in 2013, and the IEEE Industrial Electronics Society David Irwin Early Career Award in 2011 and the Bimal Bose Energy Systems Award in 2015. His industry applications have received several awards and medals, including at the Innovation Exhibition in Geneva, Switzerland, in 2006 and the Exhibition in Brussels, Belgium, "Eureco" in 2006.